Guidance and Control Law Design for a Slung Payload in Autonomous Landing: A Drone Delivery Case Study

Longhao Qian, Silas Graham, and Hugh H.-T. Liu, *Member, IEEE*

***Abstract*—This article presents a novel guidance and control design for a parcel tethered to a drone in its delivery mission. The proposed proportional-navigation-based guidance, integrated with custom-built control, enables to achieve autonomous payload landing. The novelty of the proposed method lies in two aspects: 1) the guidance law allows for soft landing and 2) the path-following control ensures the swing-free payload transportation that sets the solid foundation for landing. The development is verified by extensive simulations and further demonstrated by flight experiments.**

***Index Terms*—Autonomous landing, control, drone delivery, guidance.**

I. Introduction

AN UNMANNED aerial vehicle (UAV) is a flying system that does not carry a human pilot for operation. The popularity of these vehicles has increased drastically in the past decade, and they start to become mainstream in public applications. They are often referred to simply as "drones," but are now formally recognized in Canada as a remotely piloted aerial system. The use of UAVs has spread to many applications and sectors in recent years owing to their versatility, cost, and flexible operation characteristics. These applications range from their extensive commercial use in photography and surveying to industrial applications such as forest fire monitoring. One application that has received interest and attention in both industry and academia is the use of UAVs for payload delivery. A UAV can carry a payload in a variety of ways, which can broadly be categorized into three methods: rigidly connected to the UAV body, a cable slung payload, and a manipulator-arm carried payload. Among these choices, the slung payload configuration is the choice of this article. The slung payload configuration allows the vehicle to safely deliver the payload to the ground without the need for the vehicle to land. This may also improve the mission efficiency by allowing the vehicle to hover over the landing zone, instead of completing a full landing and takeoff procedure. However, there are difficulties associated with the slung payload configuration. For example, the position of the payload is more difficult to control accurately, because of wind, rotor downwash, and the swinging dynamics of the payload relative to the UAV. Because of these reasons, the slung payload method has generated research interest and has been extensively studied in recent years—with a focus on control, payload lifting, and swing-free trajectory tracking.

Most of the study of the UAV slung payload system focuses on designing controllers to fly along a desired trajectory. Palunko *et al.* specified a trajectory for the UAV that will minimize the payload swing during transportation along the path [1]. Kui *et al.* proposed a sliding-mode controller to track a given trajectory with the quadrotor using no explicit payload feedback, which worked well in simulation [2]. It is likely to encounter disturbances due to wind or the swinging motion of the payload. Therefore, Nicotra *et al.* proposed a controller that demonstrates some robustness to payload disturbances [3]. Qian and Liu presented a path-following controller for the slung payload system, which is robust against wind disturbances on the system [4]. Guerrero *et al.* presented a passivity-based approach to suppress the swinging motion of the slung payload while tracking a trajectory [5]–[7]. Their approach was not dependent on the swing angle, and they found that the swing motion was suppressed along the flight trajectory. In terms of landing, although research on quadrotor landing has been covered, such as [8]–[11], to the best knowledge of the authors of this article, the challenge of landing of the slung payload has not been well studied. A relevant work by Goodarzi [12] uses a variable-length cable to lower the payload to the ground shown by simulation, followed by experimentation by others using an additional payload-lowering mechanism [13].

This article presents a novel guidance and control design for a slung payload in its drone delivery mission. The proposed proportional-navigation-based guidance, integrated with custom-built control, enables to achieve autonomous payload landing. The novelty of the proposed method is shown in

Manuscript received January 8, 2020; revised March 26, 2020; accepted April 26, 2020. Date of publication June 1, 2020; date of current version August 13, 2020. This work was supported by the Natural Science and Engineering Research Council of Canada, under its Collaborative Research Program under Grant CRDPJ 508381-16, in collaboration with Drone Delivery Canada (www.dronedeliverycanada.com). Recommended by Technical Editor Y.-J. Pan and Senior Editor X. Chen. *(Corresponding author: Hugh H.-T. Liu.)*

Longhao Qian and Hugh H.-T. Liu are with the Institute for Aerospace Studies, University of Toronto, Toronto, ON M3H 5T6, Canada (e-mail: longhao.qian@mail.utoronto.ca; liu@utias.utoronto.ca).

Silas Graham is with the Institute for Aerospace Studies, University of Toronto, Toronto, ON M3H 5T6, Canada (e-mail: silas@flight.utias.utoronto.ca).

This article has supplementary downloadable material available at https://ieeexplore.ieee.org, provided by the authors.

Color versions of one or more of the figures in this article are available online at https://ieeexplore.ieee.org.

Digital Object Identifier 10.1109/TMECH.2020.2998718

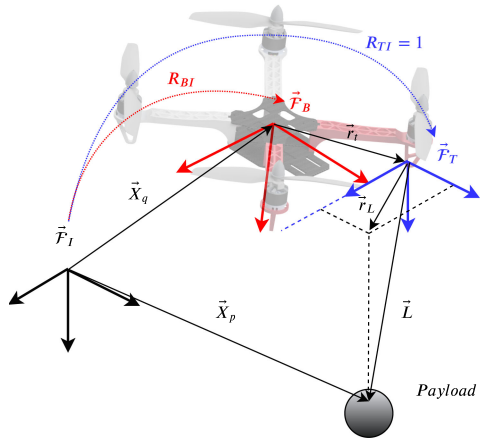

Fig. 1. Frame definition of the off-centered slung payload.

two aspects: 1) a proportional-navigation-based guidance law is designed to allow for soft landing (zero velocity when touching down) and 2) the guidance law is integrated with a path-following control, based on our previous work [4], which ensures the swing-free payload transportation that sets the solid foundation for landing. The development is verified by extensive simulations and further demonstrated by flight experiments.

II. Problem Statement

A representative UAV with the slung payload configuration is shown in Fig. 1, where the equations of motion are derived based on the multibody principle. The offset tether location means that the tether or cable is not attached at the center of mass (CM) of the vehicle, but rather at some offset distance on the vehicles frame.

The position of the payload can be described as $\vec{X}_p = \vec{X}_q + \vec{r}_t + \vec{L}$, leading to its expression in the inertial frame, denoted by the subscript I

$$\boldsymbol{X}_{p,I} = \boldsymbol{X}_{q,I} + \boldsymbol{R}_{IB}\boldsymbol{r}_t + \boldsymbol{L}_I \tag{1}$$

where $\boldsymbol{R}_{IB}$ is the rotation matrix from the inertial frame to the body frame. We make several assumptions about the modeling for the control design purpose: 1) the tether is assumed taunted all the time. It is also rigid and of fixed length, similar to the work of Qian and Liu [14]. Therefore, the motion is constrained to two degrees of rotation at the fixed tether point, at the origin of $\mathcal{F}_T$; and 2) the tether off-set distance $\boldsymbol{r}_t \approx \boldsymbol{0}$. In the actual delivery mission, the cable is attached close to the CM of the quadrotor; therefore, this is a reasonable assumption that decouples the quadrotor rotation and translation in modeling and control design. The tether is projected into the $\mathbf{t}_x$–$\mathbf{t}_y$ plane. We define the tether $\vec{L}$ in the inertial frame as $\boldsymbol{L}_I = [\boldsymbol{r}_L^T \; L_{z,I}]^T$, where $\boldsymbol{r}_L$ is the vector representing the projection of the tether into the $\mathbf{t}_x$–$\mathbf{t}_y$ plane and $L_{z,I} = \sqrt{L^2 - \boldsymbol{r}_L^T\boldsymbol{r}_L}$ due to its constraint to two (rotational) degrees of freedom (DOFs). The velocity state of the payload is obtained by taking the inertial time derivative

$$\boldsymbol{v}_{p,I} = \boldsymbol{v}_{q,I} - \boldsymbol{R}_{IB}\boldsymbol{r}_t^{\times}\boldsymbol{\omega}_B + \boldsymbol{B}\dot{\boldsymbol{v}}_L \tag{2}$$

where $\boldsymbol{\omega}_B = [p \; q \; r]^T$, and $\boldsymbol{B}$ is a kinematic relationship such that $\boldsymbol{B}\boldsymbol{v}_L = \dot{\boldsymbol{L}}_I$ and is written as follows:

$$\boldsymbol{B} = \begin{bmatrix} \mathbf{1}_{2\times 2} \\ -\dfrac{\boldsymbol{r}_L^T}{\sqrt{L^2 - \boldsymbol{r}_L^T\boldsymbol{r}_L}} \end{bmatrix}. \tag{3}$$

Again knowing that the tether position $\boldsymbol{r}_t$ is fixed on the quadrotor, we differentiate (2) to obtain the inertial payload acceleration as

$$\dot{\boldsymbol{v}}_p = \dot{\boldsymbol{v}}_q - \dot{\boldsymbol{R}}_{IB}\boldsymbol{r}_t^{\times}\boldsymbol{\omega}_B - \boldsymbol{R}_{IB}\boldsymbol{r}_t^{\times}\dot{\boldsymbol{\omega}}_B + \dot{\boldsymbol{B}}\boldsymbol{v}_L + \boldsymbol{B}\dot{\boldsymbol{v}}_L. \tag{4}$$

Here, we treat the dynamics of the quadrotor as a generic six-DOF rigid body, and the dynamics of the payload are treated as a point mass. We also apply the assumption of $\boldsymbol{r}_t \approx \boldsymbol{0}$ in the dynamics model. Using the Newton–Euler formalism yields the following dynamic equations of motion for the system:

$$m_q\dot{\boldsymbol{v}}_q = m_q\boldsymbol{g}_I + \boldsymbol{T} + \boldsymbol{F} \tag{5}$$

$$\boldsymbol{J}_q\dot{\boldsymbol{\omega}}_B = -\boldsymbol{\omega}_B^{\times}\boldsymbol{J}_q\boldsymbol{\omega}_B + \boldsymbol{M}_B \tag{6}$$

$$m_p\dot{\boldsymbol{v}}_p = m_p\boldsymbol{g}_I - \boldsymbol{T}. \tag{7}$$

$\boldsymbol{X}_T^T = [\boldsymbol{v}_L^T \;\; \boldsymbol{v}_q^T \;\; \boldsymbol{r}_L^T \;\; \boldsymbol{x}_q^T]$ is defined as the translational state. $\boldsymbol{X}_R = \{\boldsymbol{R}_{IB}, \boldsymbol{\omega}_B\}$ is defined as the attitude state. The complete state is $\boldsymbol{\mathcal{X}} = \{\boldsymbol{X}_T, \boldsymbol{X}_R\}$. Similarly, we define velocity subsets of $\boldsymbol{\mathcal{X}}$ as $\boldsymbol{V}^T = [\boldsymbol{v}_L^T \;\; \boldsymbol{v}_q^T]$. The input to the system is defined as $\boldsymbol{U}^T = [\boldsymbol{F}_I^T \;\; \boldsymbol{M}_B^T]$. We can rewrite the system equations of motion as follows:

$$\dot{\boldsymbol{\mathcal{X}}} = f(\boldsymbol{\mathcal{X}}, \boldsymbol{U}) : \begin{cases} \dot{\boldsymbol{V}} = \boldsymbol{M}^{-1}(\boldsymbol{F} + \boldsymbol{G} - \boldsymbol{C}\boldsymbol{V}) \\ \dot{\boldsymbol{x}}_q = \boldsymbol{v}_q \\ \dot{\boldsymbol{r}}_L = \boldsymbol{v}_L \\ \dot{\boldsymbol{\omega}}_B = \boldsymbol{J}_q^{-1}(-\boldsymbol{\omega}_B^{\times}\boldsymbol{J}_q\boldsymbol{\omega}_B + \boldsymbol{M}_B) \\ \dot{\boldsymbol{R}}_{IB} = \boldsymbol{R}_{IB}\boldsymbol{\omega}_B^{\times} \end{cases}. \tag{8}$$

There system matrices are defined as follows:

$$\boldsymbol{M} = \begin{bmatrix} m_p\boldsymbol{B}^T\boldsymbol{B} & m_p\boldsymbol{B}^T \\ m_p\boldsymbol{B} & (m_q + m_p)\mathbf{1}_{3\times 3} \end{bmatrix}, \quad \boldsymbol{C} = \begin{bmatrix} m_p\boldsymbol{B}^T\dot{\boldsymbol{B}} & \boldsymbol{0} \\ m_p\dot{\boldsymbol{B}} & \boldsymbol{0} \end{bmatrix}$$

$$\boldsymbol{F} = \begin{bmatrix} \boldsymbol{0} \\ \boldsymbol{F}_I \end{bmatrix}, \boldsymbol{G} = \begin{bmatrix} m_p\boldsymbol{B}^T\boldsymbol{g}_I \\ (m_q + m_p)\boldsymbol{g}_I \end{bmatrix} \tag{9}$$

where $\boldsymbol{A} = -\boldsymbol{R}_{IB}\boldsymbol{r}_t^{\times}$. The problem statement is now formulated as follows: given a target quadrotor position $\boldsymbol{x}_t$, design a feedback law $\boldsymbol{F} = \Phi(\boldsymbol{\mathcal{X}}, \boldsymbol{Z}), \dot{\boldsymbol{Z}} = \Theta(\boldsymbol{\mathcal{X}})$, such that $t \to \infty$, $\boldsymbol{x}_q \to \boldsymbol{x}_t$, $\boldsymbol{v}_q \to \boldsymbol{0}$, $\boldsymbol{v}_L \to \boldsymbol{0}$, and $\boldsymbol{r}_L \to \boldsymbol{0}$. In other words, we wish to design a proper guidance and control law, which ensures that the UAV-payload system flies along a prescribed path to reach the target landing location and makes sure when the payload is landed, its vertical touch down speed becomes zero for soft landing.

III. Guidance and Control Law Design

When considering a payload delivery mission, a critical mission segment is the landing procedure. This is the portion of the mission, where the payload goods will be delivered to the desired location on the ground. In a practical delivery application, the

payload may be fragile or have contents that should not be subjected to harsh shocks. From this perspective, it is natural to conclude that the payload should be delivered to the ground with a soft touchdown. If the payload is rigidly connected to the UAV, this implies that the UAV should have a soft contact with the ground when landing. If the payload is carried by a tether from the UAV, it is the touchdown of the payload to the ground that must be controlled. In this section, we investigate using a guidance law to achieve an autonomous landing.

A. Linearized Dynamic Model

This section presents the linearized model based on (8). According to the assumption of $\boldsymbol{r}_t \approx \boldsymbol{0}$, the translational channel is decoupled from the attitude dynamics of the quadrotor. In addition, we assume that the attitude controller provided in Section III-D responds at a much faster rate than the translational channel containing $\boldsymbol{x}_q$ and $\boldsymbol{r}_L$. Therefore, we can first design the controller for the translational channel f_T

$$\dot{\boldsymbol{X}}_T = f_T(\boldsymbol{X}_T, \boldsymbol{U}_T) : \begin{cases} \dot{\boldsymbol{V}} = \boldsymbol{M}^{-1}(\boldsymbol{F} + \boldsymbol{G} - \boldsymbol{C}\boldsymbol{V}) \\ \dot{\boldsymbol{x}}_q = \boldsymbol{v}_q \\ \dot{\boldsymbol{r}}_L = \boldsymbol{v}_L \end{cases} \tag{10}$$

where $\boldsymbol{U}_T = \boldsymbol{F}_I$. We present the following chain rule for determining the Jacobian matrix of a matrix–vector product.

Lemma 1: We define $\boldsymbol{A} \in \mathbb{R}^{N\times N}$, $x \in \mathbb{R}^{N\times 1}$, $y \in \mathbb{R}^{M\times 1}$, and $\boldsymbol{J}_y = \frac{\partial \boldsymbol{A}x}{\partial y^T}$. Then, we have the following identity:

$$\boldsymbol{J}_y = \begin{bmatrix} x^T \boldsymbol{J}_{A_1,y} \\ \vdots \\ x^T \boldsymbol{J}_{A_N,y} \end{bmatrix} + \begin{bmatrix} a_1 \boldsymbol{J}_{x,y} \\ \vdots \\ a_N \boldsymbol{J}_{x,y} \end{bmatrix} \tag{11}$$

where $a_1, \ldots, a_N$ are the row vectors of $\boldsymbol{A}$. The matrices $\boldsymbol{J}_{A_j,y}$ and $\boldsymbol{J}_{x,y}$ are defined as

$$\boldsymbol{J}_{A_j,y} = \begin{bmatrix} \frac{\partial a_{j,1}}{\partial y^T} \\ \vdots \\ \frac{\partial a_{j,N}}{\partial y^T} \end{bmatrix}, \quad \boldsymbol{J}_{x,y} = \begin{bmatrix} \frac{\partial x_1}{\partial y^T} \\ \vdots \\ \frac{\partial x_N}{\partial y^T} \end{bmatrix}. \tag{12}$$

The detailed derivation is shown in the Appendix.

The equilibrium point is picked as the origin, i.e., $\boldsymbol{X}_T = \boldsymbol{0}$, $\boldsymbol{F}_{I,e} = -(m_p + m_q)\boldsymbol{g}_I$. The Jacobian of $\boldsymbol{F} + \boldsymbol{G} - \boldsymbol{C}\boldsymbol{V}$ w.r.t $\boldsymbol{X}_T$ and $\boldsymbol{U}_T$ evaluated at the equilibrium are $\boldsymbol{J}_x$ and $\boldsymbol{J}_u$, respectively:

$$\boldsymbol{J}_x = \frac{\partial(\boldsymbol{F} + \boldsymbol{G} - \boldsymbol{C}\boldsymbol{V})}{\partial \boldsymbol{X}_T} = \begin{bmatrix} \boldsymbol{0}_{2\times 5} & -m_p g/l \boldsymbol{1}_{2\times 2} & \boldsymbol{0}_{2\times 3} \\ \boldsymbol{0}_{3\times 5} & \boldsymbol{0}_{3\times 2} & \boldsymbol{0}_{3\times 3} \end{bmatrix}$$

$$\boldsymbol{J}_u = \frac{\partial(\boldsymbol{F} + \boldsymbol{G} - \boldsymbol{C}\boldsymbol{V})}{\partial \boldsymbol{U}_T} = \begin{bmatrix} \boldsymbol{0}_{2\times 3} \\ \boldsymbol{1}_{3\times 3} \end{bmatrix}. \tag{13}$$

Note that at the equilibrium, $\boldsymbol{F} + \boldsymbol{G} - \boldsymbol{C}\boldsymbol{V} = \boldsymbol{0}$. According to Lemma 1, the linearized translational subsystem is

$$\delta \dot{\boldsymbol{X}}_T = \boldsymbol{A}_T \delta \boldsymbol{X}_T + \boldsymbol{B}_T \delta \boldsymbol{U}_T \tag{14}$$

$$\boldsymbol{A} = \begin{bmatrix} \boldsymbol{M}_1^{-1} \boldsymbol{J}_x \\ \vdots \\ \boldsymbol{M}_N^{-1} \boldsymbol{J}_x \end{bmatrix}, \quad \boldsymbol{B} = \begin{bmatrix} \boldsymbol{M}_1^{-1} \boldsymbol{J}_u \\ \vdots \\ \boldsymbol{M}_N^{-1} \boldsymbol{J}_u \end{bmatrix} \tag{15}$$

where $\delta \boldsymbol{X}_T$ and $\delta \boldsymbol{U}_T$ are perturbations of states and inputs from the equilibrium. Hence, the overall system matrices are

$$\boldsymbol{A}_T = \begin{bmatrix} \boldsymbol{A} \\ \boldsymbol{E}_0 \end{bmatrix}, \quad \boldsymbol{B}_T = \begin{bmatrix} \boldsymbol{B} \\ \boldsymbol{0}_{5\times 3} \end{bmatrix}, \quad \boldsymbol{E}_0 = \begin{bmatrix} \boldsymbol{1}_{5\times 5} & \boldsymbol{0}_{5\times 5} \end{bmatrix}. \tag{16}$$

B. Position Stabilization Law

We define a so-called virtual control force as $\boldsymbol{F}_{I,v}$, which is the lift that should be generated by the propellers and to replace $\boldsymbol{F}_I$. Based on the second assumption, we have the time-scale separation, meaning that we could first design $\boldsymbol{F}_{I,v}$ as a feedback law and then command the inner attitude control loop in Section III-D to tilt the quadrotor according to the direction of $\boldsymbol{F}_{I,v}$ to control the vehicle. The position stabilization law is then design based on a cascade form as a gain $\boldsymbol{K}$ as follows:

$$\begin{aligned} \boldsymbol{K} &= \begin{bmatrix} \boldsymbol{0}_{3\times 2} & \boldsymbol{K}_v & \boldsymbol{0}_{3\times 2} & \boldsymbol{K}_x \end{bmatrix} \\ \boldsymbol{F}_{I,v} &= -\boldsymbol{K}\delta \boldsymbol{X}_T - (m_p + m_q)\boldsymbol{g}_I \\ \boldsymbol{A}_c &= \boldsymbol{A}_T - \boldsymbol{B}_T \boldsymbol{K} \end{aligned} \tag{17}$$

where $\boldsymbol{A}_c$ is the closed-loop system matrix under the feedback gain $\boldsymbol{K}$. The position loop is a proportional-derivative-like controller that stabilizes both the quadrotor position and the payload motion. $\boldsymbol{K}_v$ and $\boldsymbol{K}_x$ are the gain matrices to be picked so that $\boldsymbol{A}_c$ is Hurwitz.

C. Pure-Proportional-Navigation-Inspired Control Law

We take inspiration from a standard pure proportional navigation (PPN) approach, e.g., [9], to create a guidance law for the current mission. We have a static landing position, and we would like the velocity to be zero when the final position is reached. We follow the inspiration from the traditional approach, but instead of using an acceleration command to track a constant velocity, we use a velocity command to "track" a constant position. In a sense, this lowers the dimension of the problem in time by one. We will also assume that the autopilot uses a position controller that we can use to control the vehicle. The intuition for this comes from the idea of reaching a zero landing velocity at the final target location. This would achieve a landing, where it is required that the quadrotor or payload touches down with minimal impact. Considering the altitude axis only, the intuition here is that we want $\dot{z}_q \Rightarrow 0$ as $z_q \Rightarrow z_t$, where $\dot{z}_q$ and z_q are the velocity and height, respectively, and z_t is the target height

$$\dot{z}_{\text{cmd}} = K_{p,z}(z_t - \delta z_q). \tag{18}$$

It is further extended for 3-D guidance, as follows:

$$\dot{\boldsymbol{x}}_{\text{cmd}} = \begin{bmatrix} \dot{x}_{\text{cmd}} \\ \dot{y}_{\text{cmd}} \\ \dot{z}_{\text{cmd}} \end{bmatrix} = \boldsymbol{K}_p(\boldsymbol{x}_t - \delta \boldsymbol{x}_q). \tag{19}$$

In order to determine the overall stability of the closed-loop system, we define an augmented system state as $\bar{\boldsymbol{X}}^T = [\delta \boldsymbol{X}_T^T \quad \boldsymbol{x}_{\text{cmd}}^T]$. By adding the PPN-guidance-inspired formula into the control law, the virtual control force should be $\boldsymbol{F}_{I,v} = \boldsymbol{K}_x \boldsymbol{x}_{\text{cmd}} - \boldsymbol{K}\delta \boldsymbol{X}_T - (m_p + m_q)\boldsymbol{g}_I$. We set $\boldsymbol{x}_t = \boldsymbol{0}$ to simplify the stability analysis. Then, the corresponding augmented closed-loop system is as follows:

$$\dot{\bar{\boldsymbol{X}}} = \boldsymbol{A}_p \bar{\boldsymbol{X}} \tag{20}$$

where the system matrices are defined as

$$\boldsymbol{A}_p = \begin{bmatrix} \boldsymbol{A}_c & \boldsymbol{B}\boldsymbol{K}\boldsymbol{E}_1 \\ \boldsymbol{E}_2 & \boldsymbol{0}_{3\times 3} \end{bmatrix}, \quad \boldsymbol{E}_1 = \begin{bmatrix} \boldsymbol{0}_{7\times 3} \\ \boldsymbol{1}_{3\times 3} \end{bmatrix}$$
$$\boldsymbol{E}_2 = \begin{bmatrix} \boldsymbol{0}_{3\times 7} & -\boldsymbol{K}_p \end{bmatrix}. \tag{21}$$

For the above equation, we can see that $\boldsymbol{K}_p$ needs to be picked so that $\boldsymbol{A}_p$ is Hurwitz. To this point, we have considered the guidance law as a mean for landing the quadrotor autonomously on the ground. However, in reality, we shall also consider the application of landing a slung payload on the ground, at a given target location. If a measurement of the payload position was available, it would be possible to estimate the state of the payload. The problem could be reformulated to attempt to directly drive the payload position to the target location. However, if the payload state information is not directly available (which could be the case in some practical implementations), we can investigate how we could directly apply the proposed guidance law. In this case, we must still assume that we have position information for the quadrotor, which is reasonable as most quadrotors have a GPS and a barometer. The idea in this case is to drive the quadrotor to a virtual target location, as shown in Fig. 2.

In this figure, we use the annotation ($'$) to denote the virtual target for the UAV. What we mean by a virtual target is a desired location for the quadrotor, where the payload will also be at its desired location. However, we must also allow the payload to swing at the final location, which is denoted by $\vec{L}'$ as opposed to the current tether $\vec{L}$. If we want the payload to reach the final location, we command the virtual target for the UAV to be directly above the desired payload target, shown in (22). Here, L represents the scalar value of the tether length. This is under defined in the inertial reference frame and assumes that the payload has no swinging motion

$$x_t' = x_t \tag{22a}$$
$$y_t' = y_t \tag{22b}$$
$$z_t' = z_t + L. \tag{22c}$$

If the payload has zero or sufficiently small swing angle, then it is trivial to see that this behaves in the same way as the quadrotor landing case. However, we must consider what effect a nonzero swing angle would have on this payload landing. Using simple trigonometric functions, we can obtain relations for the offset in the z and xy positions caused by a given swing angle. Although there are two swing angles (along the x and y axes), we use θ to represent the magnitude of the swing angle in relation to the z-axis (i.e., with components along the x and y axes). Here, $\Delta z = L - L\cos(\theta)$ and $\Delta xy = L\sin(\theta)$. Δz represents the error from the desired z position, Δxy represents the error in the xy plane. The results are tabulated as a percentage of the total length, L, and shown in Table I. From these results, we can see that the xy position accuracy is affected the most by a swing angle. For small swing angles, the z position accuracy is high. For example, if the tether length is 1 m, the error in the z position is less than 5 cm, which is also within the error of the position controller under laboratory conditions. It is possible to conclude that for small swing angles, landing of the payload should be relatively unaffected, with small inaccuracy in the xy landing position. Therefore, during the landing phase, it is desirable to maintain a small swing angle to preserve landing accuracy. We will show later in the experimental investigation that the modified PPN maintains a swing angle less than 4° during landing. This is in contrast to the unguided controller, which induces a swing angle around 14° during the landing phase.

In summary, the proposed guidance law required a solid foundation for good tracking control for payload transportation with small swing angles. It has been achieved by path-following

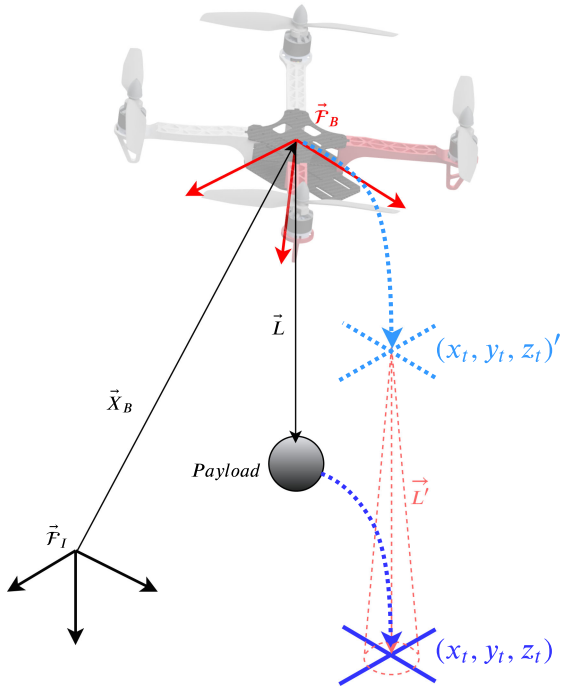

Fig. 2. Definition for the modified PPN law with a slung payload.

TABLE I
SWING ANGLE EFFECT ON PAYLOAD ACCURACY

θ [°]	Δz [% of L]	Δxy [% of L]
5	0.381	8.72
10	1.52	17.3
15	3.41	25.8

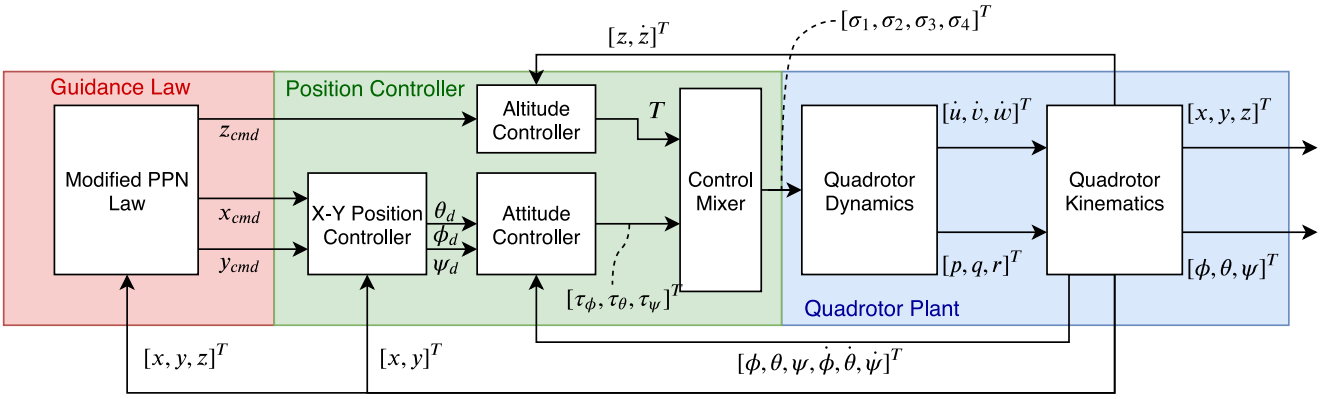

Fig. 3. Block diagram for modified PPN law implementation on a quadrotor.

control study of our research work, e.g., [4]. The overall guidance and control framework is presented by a block diagram shown in Fig. 3.

D. Attitude Controller

This section gives the target torque and lift the quadrotor should generate based on the virtual control force $\boldsymbol{F}_{I,v}$. For this type of payload manipulation control, we directly adopt an almost global asymptotically stable (AGAS) attitude tracker, as suggested in [4] . The total lift from the propellers is $f = ||\boldsymbol{F}_{I,v}||$. We pick a command yaw angle ψ for each quadrotor. We assume that lift is along the $-$z-axis of the quadrotor, i.e., $n_z = -\boldsymbol{F}_{I,v}/f$. The reference attitude trajectory of the quadrotor based on $\boldsymbol{F}_{I,v}$ is $\boldsymbol{R}_{IB,d}$ obtained in the following way:

$$\tilde{n}_x = \begin{bmatrix} \cos\psi & \sin\psi & -(\cos\psi n_{z,x} + \sin\psi n_{z,y})/n_{z,z} \end{bmatrix}^T$$
$$n_x = \tilde{n}_x/||\tilde{n}_x||, \quad n_y = n_z^\times n_x/||n_z^\times n_x||$$
$$\boldsymbol{R}_{IB,d} = \begin{bmatrix} n_x & n_y & n_z \end{bmatrix} \tag{23}$$

where $n_{z,x}$ and $n_{z,y}$ are the x and y components of n_z, respectively. $\boldsymbol{F}_{I,v}$ only provides two DOFs, i.e., n_z; therefore, ψ is an additional constraint to determine $\boldsymbol{R}_{IB,d}$. We define $\boldsymbol{\omega}_d$ as the desired angular velocity. Once $\boldsymbol{R}_{IB,d}$, $\boldsymbol{\omega}_d$, and $\dot{\boldsymbol{\omega}}_d$ are calculated based on $\boldsymbol{F}_{I,v}$, the control torque $\boldsymbol{M}_B$ is as follows:

$$\begin{aligned} \boldsymbol{M}_B = & -b_\omega\tilde{\boldsymbol{\omega}} - b_r\boldsymbol{e}_r - \tilde{\boldsymbol{\omega}}^\times\boldsymbol{J}_q\tilde{\boldsymbol{\omega}} + \boldsymbol{\omega}_B^\times\boldsymbol{J}_q\boldsymbol{\omega}_B \\ & - \boldsymbol{J}_q(\tilde{\boldsymbol{\omega}}^\times\tilde{\boldsymbol{R}}^T\boldsymbol{\omega}_d - \tilde{\boldsymbol{R}}^T\dot{\boldsymbol{\omega}}_d) \end{aligned} \tag{24}$$

where $\boldsymbol{e}_r = \sum_{i=1}^3 \boldsymbol{e}_i^\times\tilde{\boldsymbol{R}}\boldsymbol{e}_i$, $\tilde{\boldsymbol{R}} = \boldsymbol{R}_{IB,d}^T\boldsymbol{R}_{IB}$, $\boldsymbol{\omega}_d = (\boldsymbol{R}_{IB,d}^T\dot{\boldsymbol{R}}_{IB,d})^\vee$, and $\tilde{\boldsymbol{\omega}} = \boldsymbol{\omega}_B - \boldsymbol{R}_{IB}^T\boldsymbol{\omega}_d$. The propeller rotation speed can be obtained by a motor mixing algorithm in the on-board flight control unit (FCU).

IV. Gazebo Simulations

In order to evaluate design to support experimental implementation, where a PX4-based autopilot and a robot operating system (ROS) would be in the development framework for the UAV, Gazebo was selected owing to the ease of transition from simulation to experiment. Gazebo is the natural simulation tool that is used because of its compatibility and integration. The PX4 firmware that serves as the UAV's autopilot and flight controller can be run in the software-in-the-loop (SITL) mode and connected to the Gazebo physics. This means that all of the codes and algorithms executed on the hardware can be run within the simulation. This allows for easy code debugging and testing in the simulation environment prior to deployment on the experimental UAV. For this article, a custom model for the Gazebo simulator was developed based on our experimental quadrotor (F330). This model was based on a prebuilt and available model (3DR Iris); however, it was modified to match our experimental platform (from computer-aided design) and other measurements (mass and inertia), seen in Fig. 4. The model was also extended to include our laboratory room as the flight zone for testing and a slung tether payload.

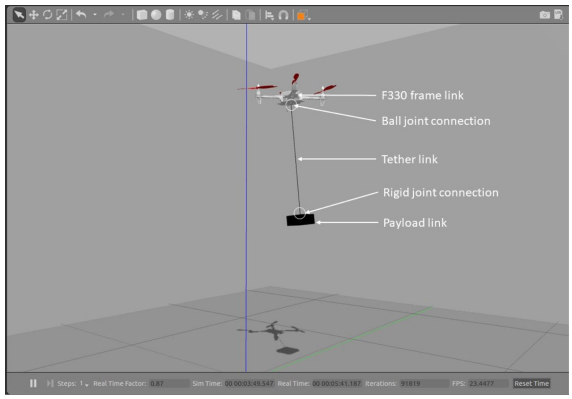

Fig. 4. Simulation in the Gazebo environment running PX4 SITL and ROS.

The principal moments of inertia around the x, y, and z axes were then calculated using the parallel axis theorem. The result from this component build-up method is $\boldsymbol{J}_q = \text{diag}([0.0115 \quad 0.0116 \quad 0.0128])[\text{kg}\cdot\text{m}^2])$. The total mass of the experimental F330 quadrotor with all components was 1.00 kg. These values were entered into the Gazebo SDF file for the F330.

TABLE II
EIGENVALUES OF $\boldsymbol{A}_p$

$\lambda_{1,2}$	$-0.0844 \pm 3.8455i$
$\lambda_{3,4}$	$-0.0111 \pm 0.5073i$
λ_5	-0.3091
$\lambda_{6,7}$	$-0.0844 \pm 3.8455i$
$\lambda_{8,9}$	$-0.0111 \pm 0.5073i$
λ_{10}	-0.3090
$\lambda_{11,12}$	$-0.0123 \pm 0.5089i$
λ_{13}	-0.3088

A. Parameter Selection and Closed-Loop Eigenvalues

After plugging in the system parameters, we have the following matrix for the linearized system:

$$\boldsymbol{A} = \begin{bmatrix} \boldsymbol{0}_{1\times5} & -14.7150 & 0 & 0 & 0 & 0 \\ \boldsymbol{0}_{1\times5} & 0 & -14.7150 & 0 & 0 & 0 \\ \boldsymbol{0}_{1\times5} & 4.9050 & 0 & 0 & 0 & 0 \\ \boldsymbol{0}_{1\times5} & 0 & 4.9050 & 0 & 0 & 0 \\ \boldsymbol{0}_{1\times5} & 0 & 0 & 0 & 0 & 0 \end{bmatrix}$$

$$\boldsymbol{B} = \begin{bmatrix} -1.0000 & 0 & 0 \\ 0 & -1.0000 & 0 \\ 1.0000 & 0 & 0 \\ 0 & 1.0000 & 0 \\ 0 & 0 & 0.6667 \end{bmatrix}. \tag{25}$$

For the control and PPN gains, we pick them as

$$\boldsymbol{K} = \begin{bmatrix} \boldsymbol{0}_{3\times2} & 0.5 \times \boldsymbol{1} & \boldsymbol{0}_{3\times2} & 0.4 \times \boldsymbol{1} \end{bmatrix}. \tag{26}$$

$\boldsymbol{K}_p = k \times \boldsymbol{1}_{3\times3} = 0.3 \times \boldsymbol{1}_{3\times3}$ is picked for the following simulation and experiments. The eigenvalues of $\boldsymbol{A}_p$ are listed in Table II. From the table, we can see that all eigenvalues are on the left-hand side of the imaginary plane. $\boldsymbol{A}_p$ is Hurwitz so that the overall closed-loop system is asymptotically stable. The virtual control force $\boldsymbol{F}_{I,v}$ is converted into a target quaternion and thrust command to the drone. For the simulation and experiment, we directly rely on the default PX4 firmware for attitude stabilization in the offboard mode.

B. Case 1: Vertical Descent

For the first case, we perform a simple vertical landing maneuver. This represents a case where the quadrotor is hovering directly over the desired landing target and allows us to evaluate the touchdown. For the sample mission, we begin hovering at a height of 4 m above the target. It should also be noted that although the x and y PPN guidance is active, they will not be discussed here, as they only keep the quadrotor at the current x and y positions during landing.

Fig. 5 shows the z position as a function of time during the landing maneuver. We also test a proportional–integral–derivative (PID) setpoint controller as our baseline (the "no PPN" case). In each case, landing is initiated by switching to the desired target position located at 0 m (i.e., a step input). It should be noted that the PID controller is also used as the inner-loop position controller for the PPN guidance law—without modification. From Fig. 5, we see that each law will eventually drive the quadrotor to land. The step input for the unguided controller results in a profile, where the quadrotor drops from the sky and crash-lands (visually observed in simulation). However, it does recover and shows a small oscillation before eventually landing. Although the controller gains might be changed to improve this landing condition, those gains may not be suitable for general position holding functionality. In contrast, we see that for the PPN gains tested, the landing maneuver is more docile and smooth.

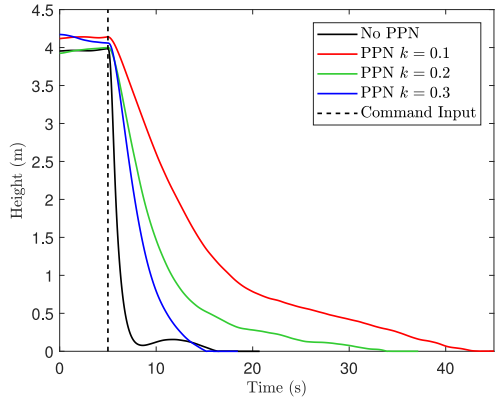

Fig. 5. Height of the quadrotor during the landing command.

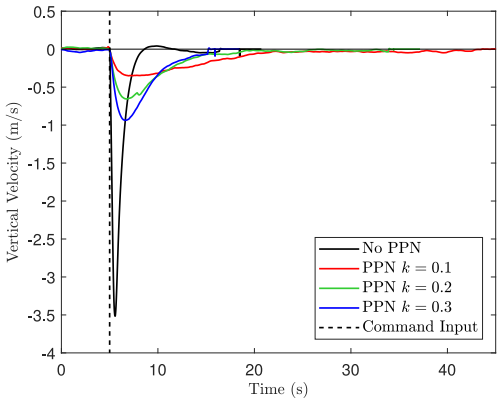

Fig. 6. z velocity of the quadrotor during the landing command.

Fig. 6 shows the vertical velocity during landing. Here, we notice the potential concern with directly using a step input for the unguided position controller when landing the vehicle. For the landing maneuver, we would like the quadrotor to move smoothly, which is not observed because of the sharp velocity profile (which corresponds to a high acceleration). Using the PPN law, we find that the velocity profile is more controlled, and the maximum velocity is kept at less than one-third that of the unguided controller.

C. Case 2: Translational Descent

For the second case, we will consider a translational descent landing maneuver for the quadrotor. This would represent a case

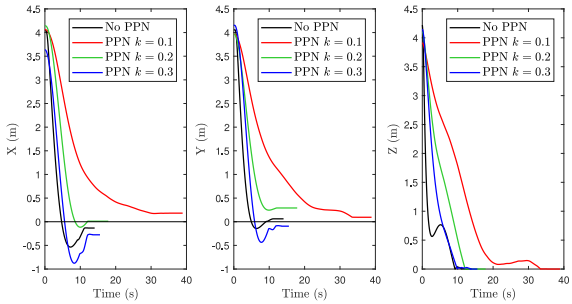

Fig. 7. x, y, and z positions of the quadrotor during landing command.

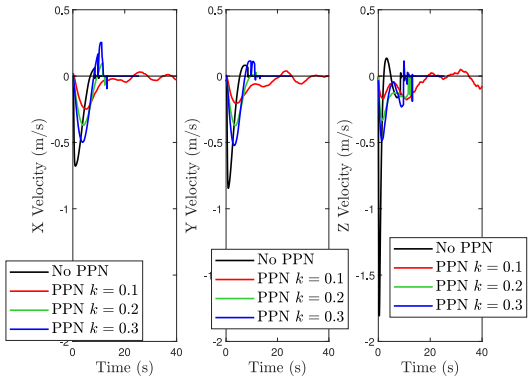

Fig. 8. x, y, and z velocities of the quadrotor during the landing command.

where the landing maneuver is initiated once the UAV is within a certain vicinity of the landing target. This allows us to evaluate the xy performance of the PPN law. The initial position of the quadrotor is set at $(x, y, z) = (4, 4, 4)$ m, and the target location is set at $(x, y, z) = (0, 0, 0)$ m.

For this case, we show the x, y, and z positions of the quadrotor as a function of time in Fig. 7. The results from this figure demonstrate a similar behavior to that observed during Case 1. Specifically, the unguided controller is fast to react to the step input, but introduces some oscillation and overshoot in the x and y axes. It should be noted that for the x and y axes, we also notice some overshoot in the PPN law, primarily at the largest gain of $k = 0.3$. In each case, there is some relatively small errors in the final xy position of the quadrotor; however, all arrive within close proximity to the desired target.

The velocities of the vehicle are shown in Fig. 8. Once again, we observe the large spike in the unguided controller velocity, indicating a very aggressive maneuver with high acceleration. This is not our desired intent for the landing maneuver, as we would like a smooth trajectory. We notice that the PPN velocities are less than one-third of the unguided controller velocities. This is again achieved with a near identical landing time as the PID control, with the PPN at $k = 0.3$. The noisy velocity behavior at the end of the trials is explained by the vehicle coming into contact with the ground. The motors are not disarmed immediately upon contact with the ground, and therefore, owing to the small offsets in the xy landing positions

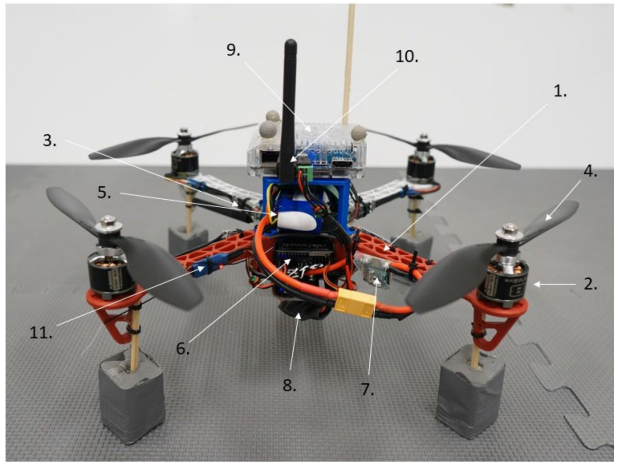

Fig. 9. F330 Quadcopter platform. 1. F330 frame, 2. NTM PropDrive 1200-kV motors, 3. LittleBee 20A ESCs, 4. 8×4.5 Propellers, 5. Turnigy 3S 2200 25C LiPo battery, 6. Pixhawk autopilot, 7. Pixhawk power module, 8. 5-V/5-A external BEC, 9. Odroid XU4, 10. WiFi adapter, and 11. FrSky XM Plus receiver.

from the desired target, the PID and PPN continue to try to reach the final desired xy position. This results in the vehicle skimming in contact with the ground, creating a noisy velocity profile around zero. To prevent this, once the quadrotor has touched down, it should be disarmed immediately (either manually or automatically through detection of this state).

V. Experimental Investigation

The assembled quadrotor with labeled components can be seen in Fig. 9. For the autopilot system on this quadrotor, we use a Pixhawk running the PX4 flight stack firmware. The Odroid XU-4 is used as an on-board computer, which runs Ubuntu 18.04 and ROS. The XU-4 is a single board computer, equipped with Samsung Exynos5422 Cortex-A15 2 GHz and Cortex-A7 octa-core CPUs. This computer is used to communicate with the ground station and Pixhawk, while providing a computational platform to implement high-level controls and algorithms. We use this on-board computer to run the guidance law and the position controller for this landing mission.

The experimental investigation for this article was completed in a laboratory environment, shown in Fig. 10. Fourteen Flex13 OptiTrack cameras[1] are used to cover the room, giving us a flyable volume of approximately $5.5 \times 3.5 \times 2.5$ m^3. The Flex13 cameras then connect to a computer via USB, which is running OptiTrack's Motive software. This software can then be used to stream the pose information of the trackable objects over a network interface using the `VRPN` interface. In our particular case presented here, we connect the computer to an ASUS AC5300 WiFi router via an Ethernet cable, for reliable connection. The OptiTrack data can then be wireless streamed from the Odroid using a 5-GHz WiFi adapter plugged into a USB port on

[1][Online]. Available: https://v22.wiki.optitrack.com/index.php?title=Calibration#Calibration_Summary

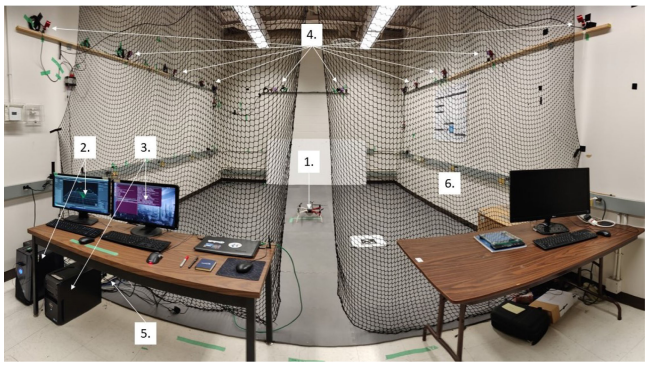

Fig. 10. Laboratory environment and setup for experiments. 1. experimental quadcopter, 2. computer running Motive software, 3. ground station computer, 4. OptiTrack Flex13 cameras, 5. (hidden) WiFi router, and 6. safety netting.

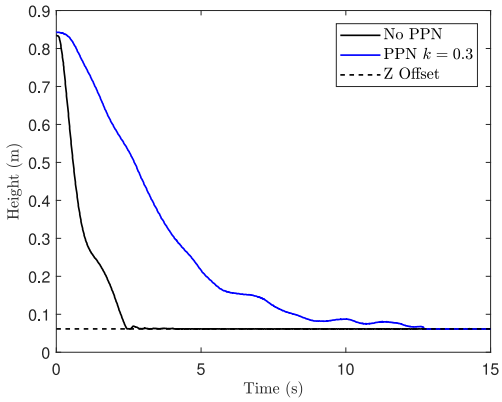

Fig. 11. Height of the payload during the landing command.

the Odroid. A 2.4-GHz connection can also be used; however, since the transmission distance is short, a 5-GHz connection is preferable.

A. Case 3: Slung Payload—Vertical Landing

Now, we will move on to the slung payload delivery mission. In this case and the following case, we use a mass of 500 g for the payload and a tether length of 1 m. The payload mass is half the mass of the experimental quadrotor; therefore, this is considered a heavy payload for the UAV. We use a heavy payload mass, as it is more likely to cause the system to be unstable. Any payload swing will have a greater effect on the quadrotor motion, due to the larger reaction forces generated through the tether. We again begin with a case where we perform a vertical landing mission. This test will evaluate the vertical landing performance of the PPN guidance law. It is important to note that for the slung payload cases, we only evaluate the PPN with a gain of $k = 0.3$, which was observed to provide the best performance from the results in Cases 1 and 2.

The time history of the payload height during the landing procedure is shown in Fig. 11. Here, we observe that the unguided controller reaches the final target faster than the PPN guided law. The steep slope for the unguided landing indicates

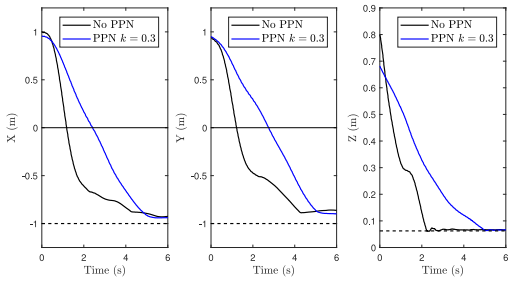

Fig. 12. x, y, and z positions of the payload during the landing command.

that the payload touched down with a higher velocity when compared to the PPN landing. This resulted in a small rebound in height resulting from the ground contact. The magnitude of this rebound is small; however, this could be due to the low initial altitude of the payload. If the payload could be flown higher, we might expect to see a more significant rebound upon touchdown. The PPN landing takes longer to finally touch down; however, the slope approaching this target is low, indicating a softer touchdown. The experiment result with the PPN law is also shown in a video.[2]

B. Case 4: Slung Payload—Translational Landing

In the final case, we perform a mission where we deliver a slung payload by performing a translational landing. This is a combination of Cases 2 and 3 to evaluate the PPN-modified guidance law for a more realistic payload delivery mission. We will again fly the quadrotor at an initial position of $(x, y, z) = (1, 1, 2)$ m. This results in a payload initial location of $(x, y, z) = (1, 1, 0.85)$ m. The quadrotor is given a virtual landing target as the goal location for delivering the payload. The virtual target location for the quadrotor is given as $(x, y, z) = (-1, -1, 1)$ m. The position of the payload during landing is shown in Fig. 12. The results show that the PPN achieved equal or better final accuracy in the x and y axes. In addition, the PPN law slowed the payload down in the z-axis and achieved a soft touchdown. However, the unguided controller essentially dropped the payload on the ground and did not achieve a soft touchdown. During the unguided controller test, touchdown occurred before the payload had reached the final goal location, which is shown more clearly in Fig. 13.

In Fig. 13, we can observe the path of the payload in the xz and yz planes, respectively. The PPN-guided landing follows a more direct path to the goal, arriving at the target along a nearly straight line. It is shown in these plots, however, that we clearly observe an issue with the unguided controller for this mission. As mentioned, the payload not only has a steep descent directly into the ground (resulting in a hard landing), but also touches down before the target location has been reached in the x and y directions. This results in the quadrotor dragging the payload along the ground until it reaches the desired x and y targets. This

[2][Online]. Available: https://youtu.be/lnX3RhOztgg

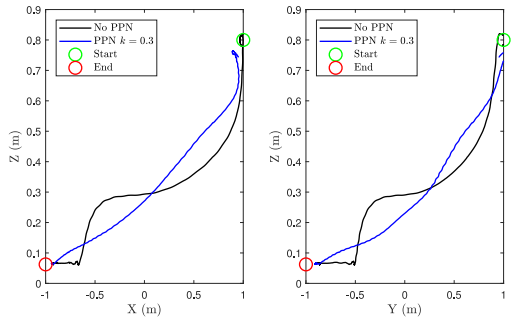

Fig. 13. xz and yz position plots of the payload.

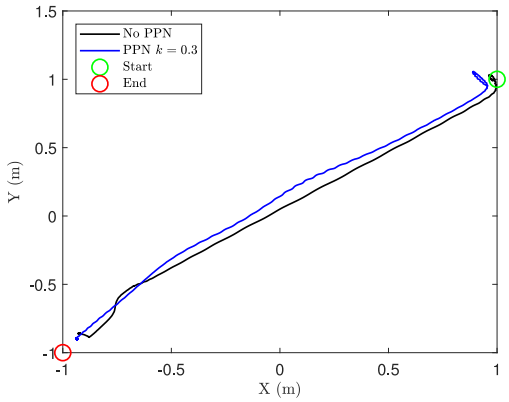

Fig. 14. xy position plot of the quadrotor.

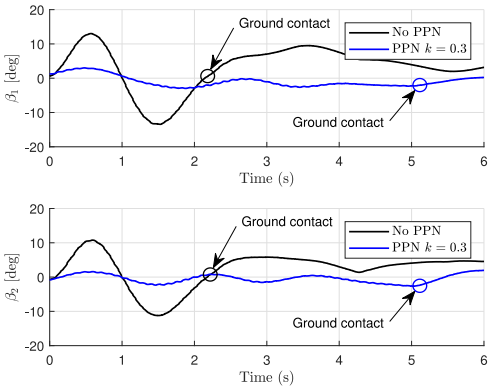

Fig. 15. Swing angles of the payload during landing.

is clearly not what could be classified as a desirable autonomous landing, with a smooth and precise touchdown.

Fig. 14 shows the x and y positions of the payload throughout the flight. In this case, we see that both the unguided and PPN-guided landings followed a reasonably straight line path to the target location along the x and y axes.

Finally, we plot the swing angles of the payload during this landing segment, shown in Fig. 15. We use two angles β_1 and β_2 to describe the two axes of swing motion for the payload. In this figure, we observe the concern with the unguided landing, as it results in a large swing angle relative to the PPN-guided landing. This results from the large initial acceleration of the quadrotor, which induces the initial swing angle. The swing angle in the unguided case reaches close to 14°, whereas the PPN-guided landing keeps the swing angle below 4°. By keeping the swing angle low, the dynamics of the UAV are less disturbed by the payload motion. This also helps in maintaining an accurate landing. We note the points at which the payload came into contact with the ground, as this stopped the free-swinging motion of the payload. The experiment result with the PPN law is also shown in a video.[3]

VI. Conclusion

In this article, we explored the emerging application of delivering payloads using a UAV. There are various methods in which this type of delivery can be performed; however, in this article, we investigated the concept of slung payload delivery. This is where the payload is attached like a pendulum to the UAV through the use of a cable or tether. The proposed guidance and control framework focused on the landing portion of the mission. We described the autonomous landing, where the aim is to deliver the payload (or UAV) to the ground with close to zero velocity at touchdown. The pure proportional-inspired guidance law, together with custom path-following control, enables the soft landing. The comparative study through extensive simulations and representative experimental investigation verified the effectiveness of the proposed approach.

Appendix
Sketch of the Proof of Lemma 1

The Jacobian $\boldsymbol{J}_y$ of the product Ax is

$$\boldsymbol{J}_y = \begin{bmatrix} \frac{\partial a_1 x}{\partial y^T} \\ \vdots \\ \frac{\partial a_N x}{\partial y^T} \end{bmatrix} \tag{27}$$

where a_j, $j = 1, 2, \ldots, N$, are the row vectors of $\boldsymbol{A}$. We define $J_{y,j}$ as the jth row vector of $\boldsymbol{J}_y$. Hence, we have

$$J_{y,j} = \frac{\partial a_j x}{\partial y^T} = \sum_{i=1}^{N} \frac{\partial a_{j,i} x_i}{\partial y^T} = \sum_{i=1}^{N} x_i \frac{\partial a_{j,i}}{\partial y^T} + a_{j,i} \frac{\partial x_i}{\partial y^T}. \tag{28}$$

Rearranging the above equation, we have

$$J_{y,j} = \begin{bmatrix} x_1, \ldots, x_N \end{bmatrix} \begin{bmatrix} \frac{\partial a_{j,1}}{\partial y^T} \\ \vdots \\ \frac{\partial a_{j,N}}{\partial y^T} \end{bmatrix} + \begin{bmatrix} a_{j,1}, \ldots, a_{j,N} \end{bmatrix} \begin{bmatrix} \frac{\partial x_1}{\partial y^T} \\ \vdots \\ \frac{\partial x_N}{\partial y^T} \end{bmatrix}. \tag{29}$$

Then, the conclusion is verified if we write $\boldsymbol{J}_y$ in matrix format.

Acknowledgment

The authors would like to express appreciation to the following DDC technical and management staff for their continuous support: Paul Di Benedetto, Greg Colacitti, Erik Chau, Rikky Duivenvoorden, and Yih Tang Yeo.

[3][Online]. Available: https://youtu.be/fGq2gfyumcU

REFERENCES

[1] I. Palunko, R. Fierro, and P. Cruz, "Trajectory generation for swing-free maneuvers of a quadrotor with suspended payload: A dynamic programming approach," in *Proc. IEEE Int. Conf. Robot. Autom.*, 2012, pp. 2691–2697.

[2] Y. Kui, G. Feng, Y. Liying, H. Yuqing, and H. Jianda, "Sliding mode control for a quadrotor slung load system," in *Proc. 36th Chin. Control Conf.*, 2017, pp. 3697–3703.

[3] M. M. Nicotra, E. Garone, R. Naldi, and L. Marconi, "Nested saturation control of an UAV carrying a suspended load," in *Proc. Amer. Control Conf.*, 2014, pp. 3585–3590.

[4] L. Qian and H. H. T. Liu, "Path following control of a quadrotor UAV with a cable suspended payload under wind disturbances," *IEEE Trans. Ind. Electron.*, vol. 67, no. 3, pp. 2021–2029, Mar. 2020.

[5] M. E. Guerrero, D. A. Mercado, R. Lozano, and C. D. García, "IDA-PBC methodology for a quadrotor UAV transporting a cable-suspended payload," in *Proc. IEEE Int. Conf. Unmanned Aircr. Syst.*, 2015, pp. 470–476.

[6] M. E. Guerrero, D. A. Mercado, R. Lozano, and C. D. García, "Passivity based control for a quadrotor UAV transporting a cable-suspended payload with minimum swing," in *Proc. 54th IEEE Conf. Decis. Control*, 2015, pp. 6718–6723.

[7] M. E. Guerrero-Sánchez, D. A. Mercado-Ravell, R. Lozano, and C. D. García-Beltrán, "Swing-attenuation for a quadrotor transporting a cable-suspended payload," *ISA Trans.*, vol. 68, pp. 433–449, 2017.

[8] Z. Shi and L. Zhao, "On the autopilot design for a quadrotor during landing phase," in *Proc. IEEE 35th Chin. Control Conf.*, 2015, pp. 10875–10879.

[9] A. Gautam, P. B. Sujit, and S. Saripalli, "Application of guidance laws to quadrotor landing," in *Proc. IEEE Int. Conf. Unmanned Aircr. Syst.*, 2015, pp. 372–379.

[10] C. Luo, W. Zhao, Z. Du, and L. Yu, "A neural network based landing method for an unmanned aerial vehicle with soft landing gears," *Appl. Sci.*, vol. 9 no. 15, 2019, Art. no. 2976.

[11] M. F. Sani, M. Shoaran, and G. Karimian, "Automatic landing of a low-cost quadrotor using monocular vision and Kalman filter in GPS-denied environments," *Turkish J. Elect. Eng. Comput. Sci.*, vol. 27 no. 3, pp. 1821–1838, 2019.

[12] F. A Goodarzi, "Autonomous aerial payload delivery with quadrotor using varying length cable," in *Proc. IEEE Int. Conf. Adv. Mechatronic Syst.*, 2016, pp. 394–399.

[13] W. G. Patrick, J. R. Burgess, and A. Conrad, "Mechanisms for lowering a payload to the ground from a UAV," U.S. Patent 9 783 297, Oct. 10, 2017.

[14] L. Qian and H. H. T. Liu, "Dynamics and control of a quadrotor with a cable suspended payload," in *Proc. IEEE 30th Can. Conf. Elect. Comput. Eng.*, 2017, pp. 1–4.

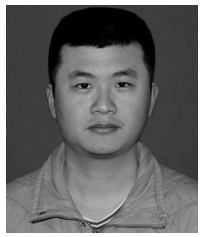

Longhao Qian received the bachelor's degree in aeronautics and astronautics engineering from Shanghai Jiao Tong University, Shanghai, China, in 2013. He is working toward the Ph.D. degree with the Institute for Aerospace Studies, University of Toronto, Toronto, ON, Canada.

His research interests include cooperative drone stability and control.

Silas Graham received the master of applied science degree in aerospace science and engineering from the Institute for Aerospace Studies, University of Toronto, Toronto, ON, Canada, in 2019.

His research interest includes drone delivery project.

Hugh H.-T. Liu (Member, IEEE) received the bachelor's degree in automation science and engineering from Shanghai Jiao Tong University, Shanghai, China, in 1991, the master's degree in electrical and automation engineering from the Beijing University of Aeronautics and Astronautics, Beijing, China, in 1994, and the Ph.D. degree in mechanical engineering from the University of Toronto, Toronto, ON, Canada, in 1998.

He is currently a Professor with the Institute for Aerospace Studies, University of Toronto. His research interests include autonomous unmanned systems, cooperative and formation control, fault-tolerant control, active control on advanced aircraft systems, and integrated modeling and simulations.

Dr. Liu has served many years as a Member of the Guidance, Navigation, and Control Technical Committee of the American Institute of Aeronautics and Astronautics (AIAA). He is an Associate Editor for the *AIAA Journal of Guidance, Control and Dynamics* and the *Canadian Aeronautics and Space Journal*. He is an Associate Fellow of the AIAA and the Canadian Society of Mechanical Engineers and a Registered Professional Engineer in Ontario, Canada.